# Discrimination of C1:G72 Microhelix$^{Ala}$ by AlaRS Is Based on Specific Atomic Groups Rather Than Conformational Effects: An NMR and MD Analysis

**Deborah A. Kallick,*,†,‡ Maria C. Nagan,§ Penny J. Beuning,§,|| Stephanie Kerimo,§ Michael R. Tessmer,†,⊥ Christopher J. Cramer,§ and Karin Musier-Forsyth*,§,#**

*Department of Medicinal Chemistry and Department of Chemistry and Supercomputer Institute, University of Minnesota, Minneapolis, Minnesota 55455*

*Received: April 11, 2002*

The acceptor stem domain of tRNA$^{Ala}$ contains the major recognition elements for aminoacylation by *Escherichia coli* alanine−tRNA synthetase (AlaRS). Previous studies established that a simple base pair transversion (G1:C72 → C1:G72) completely abolishes in vitro aminoacylation with alanine of duplex$^{Ala}$ substrates. Subsequent atomic group "mutagenesis" experiments, wherein over 30 base pair variants were introduced at this site, revealed that the presence of a major groove carbonyl oxygen at position 72 functions as a negative determinant. Although, these previous biochemical studies strongly suggested the critical nature of a blocking element at this site, they could not rule out the possibility that conformational changes were responsible for the observed effects on aminoacylation. The mechanism of discrimination at the first base pair is further examined here. In particular, to establish whether conformational change contributes to the striking difference in aminoacylation activity, NMR spectroscopy and molecular dynamics (MD) simulations were carried out. The solution NMR assignments indicate that the global conformations of the wild-type microhelix versus the C1:G72-containing variant are very similar. This is consistent with the predicted structures based on MD simulations; on the basis of average structures and dynamical analysis of trajectories, there are no statistically significant differences between the variant and the wild-type microhelices with respect to either helical structure or A73 stacking interactions. Thus, AlaRS is indeed sensitive to specific atomic groups in the inactive C1:G72 variant rather than to conformational changes associated with this base pair transversion.

## Introduction

Each member of the family of proteins known as the aminoacyl−tRNA synthetases must select their cognate tRNA substrates from among more than sixty cellular tRNAs. Because all tRNAs are known to fold into a similar global tertiary structure, the molecular basis for this discrimination is not immediately obvious. Aminoacyl−tRNA synthetases use a set of positive recognition elements as well as additional negative elements to achieve the remarkable discrimination necessary to maintain the fidelity of protein translation.[1] As an example, biochemical studies performed using the *Escherichia coli* alanine system have revealed that major positive recognition elements include an array of minor groove functional groups in and around a critical G3:U70 wobble base pair.[2−5] The N7 of A73 is another positive recognition element for alanine−tRNA synthetase (AlaRS),[6] and this so-called "discriminator base" has been shown by solution NMR to stack over the G1 of the first base pair.[7] Recent molecular dynamics (MD) simulations indicate that there is a positive correlation between N73 base stacking propensity and aminoacylation activity.[8]

Negative elements that decrease in vitro aminoacylation with alanine have also been identified. For example, a base pair transversion (G:C → C:G) at 1:72 completely abolishes in vitro aminoacylation with alanine of duplex$^{Ala}$ substrates.[9] Over 30 base pair combinations were incorporated at this site and it was discovered that the atomic groups in the wild-type G1:C72 pair do not contribute significantly to positive recognition.[10] Instead, a major groove carbonyl oxygen at position 72 was identified as a blocking element.[10,11] The mechanism of this blocking effect may be through direct unfavorable interactions with the enzyme or via an indirect conformational effect. To distinguish between these two possibilities, additional structural information is needed.

Circular dichroism spectroscopy has already established that the wild-type and inactive C1:G72 duplexes have similar secondary structures.[10] However, this method is ill-suited to probe tertiary structural differences in the conformation of the ACCA$^{76}$-3′ end, or to detect subtle differences in base stacking. Our recent data indicate that AlaRS aminoacylation activity is indeed sensitive to alterations in stacking interactions between A73 and the first base pair.[8] Moreover, sequence-dependent changes in the conformation of the NCCA$^{76}$-3′ end of microhelices that differ only at position 73 have previously been observed by solution NMR.[12−14] Given the proximity of the first base pair to N73, a base known to influence acceptor stem conformation, as well as AlaRS's sensitivity to conformational changes in this region, it was important to establish whether significant differences in stacking interactions and/or other more global conformational differences exist between the wild-type and C1:G72 duplexes. Here, we use NMR spectroscopy and

* Corresponding authors. E-mail: dkallick@incyte.com; musier@chem.umn.edu.

† Department of Medicinal Chemistry.

‡ Current address: Incyte Genomics, Inc., 2160 Porter Drive, Palo Alto, CA 94304.

§ Department of Chemistry and Supercomputer Institute.

|| Current address: Department of Biology 68-653, Massachusetts Institute of Technology, 77 Massachusetts Avenue, Cambridge, MA 02139.

⊥ Current address: Department of Chemistry, Southwestern College, 100 College Street, Winfield, KS 67156.

# Mailing address: Department of Chemistry, 207 Pleasant Street SE, 139 Smith Hall, Minneapolis, MN 55455-0431.

10.1021/jp020956r CCC: $22.00 
Published on Web 08/02/2002

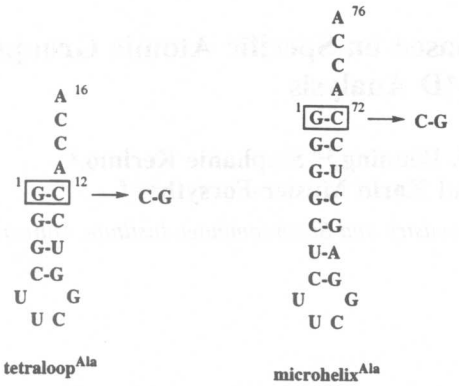


**Figure 1.** Sequence of RNAs examined in this study. The arrow points to the mutation made in the first base pair (boxed). RNAs are derived from the acceptor stem of *E. coli* tRNA$^{Ala}$. The first base pair in full-length tRNA$^{Ala}$ is at position 1:72, and this numbering convention is maintained for the microhelix$^{Ala}$ studied by MD simulation (right). A shorter 16-mer tetraloop$^{Ala}$ was used in NMR studies (left), and the first base pair in this case is at position 1:12.

MD simulations to probe conformational differences between the wild-type G1:C72-containing RNA and the inactive C1:G72 variant. We find no major conformational or stacking differences between these RNAs. These results together with extensive biochemical analysis of base pair variants at this site, allow us to conclude that it is functional group differences that are most important in discrimination at the first base pair of tRNA$^{Ala}$.

## Materials and Methods

**RNA Preparation.** RNAs for NMR analysis (wild-type tetraloop$^{Ala}$ and C1:G12 variant, Figure 1; the nucleotide numbering convention used throughout this work is described in the legend to Figure 1) were synthesized using the phosphoramidite method on a Gene Assembler Special (Pharmacia). Ultrahigh purity acetonitrile and dichloroethane were obtained from VWR. RNA phosphoramidite monomers were purchased from Chemgenes (Waltham, MA). All other RNA synthesis chemicals and the controlled pore glass solid supports were from Glen Research (Sterling, VA). Buffers were prepared using diethylpyrocarbonate-treated water.[15] Chemically synthesized RNA was deprotected, gel purified on denaturing 16% polyacrylamide gels, eluted, and desalted as described.[16,17] For NMR analysis, the RNA was further purified by extensive buffer exchange with the NMR buffer (100 mM NaCl, 10 mM $NaPO_4$, pH 6.2) as previously described.[18]

**Nuclear Magnetic Resonance Spectroscopy.** NMR data were collected on Varian Inova spectrometers operating at proton frequencies of 600 and 800 MHz unless otherwise noted. The majority of the protons were assigned by homonuclear methods using literature procedures. Two-dimensional NOE spectra[19] were collected at 5, 10, 15, 20, and 30 °C, with mixing times of 50, 75, 100, 150, 200, 250, 300, and 400 ms. Data were processed with nmrpipe and sparky. NOESY spectra were also collected sequentially to allow NOE buildup information to be extracted. DQF-COSY and TOCSY spectra were collected as appropriate. $^{1}H-^{13}C$ HMQC spectra were collected at 800 MHz for proton and 212 MHz for carbon. The carbon assignments were used to unambiguously distinguish between H2 and H8 protons. T1 relaxation experiments were carried out at 600 MHz and were used to support the H2 assignments obtained from the HMQC.

**Molecular Dynamics Simulations.** MD simulations of the wild-type RNA microhelix$^{Ala}$ and the C1:G72 variant (Figure 1) were performed as described previously.[20] Initial structures for the simulations were derived from a high-resolution NMR structure of wild-type *E. coli* microhelix$^{Ala}$.[7] Simulations employed the Cornell et al.[21] force field as implemented in AMBER 5.0.[22] The microhelices were surrounded by sodium counterions and 9 Å of TIP3P water.[23] A particle mesh Ewald formalism was used to account for long-range electrostatics.[24] Simulations were carried out using the SANDER module of AMBER 5.0 with a 2.0-fs time step. The SHAKE algorithm[25] was applied to all hydrogen atoms and the Lennard-Jones cutoff was set to 9.0 Å. The pairlist was updated every 25 steps. Constant pressure (1 bar) and temperature (300 K) were maintained according to the Berendsen coupling algorithm.[26] The detailed equilibration protocol of Cheatham was employed,[27] except that all simulations were equilibrated for an additional 500 ps prior to collection of production statistics. The CARNAL module of AMBER 5.0 and the Curves 5.3 program[28] for helical parameters were used to analyze the trajectories. Structures and movies of trajectories were visualized using Insight[29] and VMD.[30] Properties were averaged over 2000 snapshots taken every 1 ps of the 2.0 ns simulation.

We generated three different trajectories for use in our analysis. The first, called wild-type simulation A, is a 2-ns trajectory for the wild-type microhelix. A second wild-type trajectory of 1 ns was also generated using a different random seed for comparison purposes, and this is called wild-type simulation B. Finally, a 2-ns trajectory for the C1:G72 variant was also generated. Comparisons made between any pair of average structures from these three simulations involve initial optimized overlay of *only* the duplex region that is conserved among all three, i.e., from 2:71 to 7:66.

## Results

**NMR Analysis of Wild-Type Tetraloop$^{Ala}$ and a C1:G12 Variant.** Homonuclear 2D NMR assignments of the 16-mer wild-type tetraloop$^{Ala}$ and the C1:G12 variant (Figure 1, left) proceeded generally according to published procedures. The structure of the 22-mer wild-type microhelix$^{Ala}$ (Figure 1, right) was previously determined to high resolution with $^{15}N$ and $^{13}C$ labels.[7] Although this assisted somewhat in our assignments of the shorter constructs, resonances of the wild-type 16-mer differed slightly from those of the published microhelix$^{Ala}$, presumably due to the differences in the lengths of the two helices. Thus, completion of the wild-type tetraloop$^{Ala}$ assignments by homonuclear methods was essential for comparison to the mutant C1:G12 variant. The homonuclear assignments of the latter construct presented considerable challenges. The spectra shown in Figure 2 represent the optimal temperature (15 °C) and field (800 MHz) for homonuclear NMR of the two RNAs. Nearly all of the proton resonances were assigned, with some expected ambiguity remaining with the H5′, H5″ protons (table of complete chemical shifts provided in Supporting Information). At most temperatures, there were three key resonances that were overlapped in the C1:G12 variant: A13H8, G12H8, and C4H6. These resonances were resolved using the conditions described in Figure 2.

Several resonances have significantly different chemical shifts in the mutant RNA relative to the wild-type (Figure 2). In particular, the chemical shift of A13H8 is well upfield in the mutant (7.52 ppm) relative to the wild-type (7.88 ppm). The A13H2 chemical shift changes by a still larger margin, from 7.06 ppm in the wild-type RNA to 7.58 in the mutant. These assignments were complicated by the fact that the A13H2 in the mutant RNA is degenerate with the C15H6 at most temperatures and magnetic fields; moreover, the C1H1′ chemical

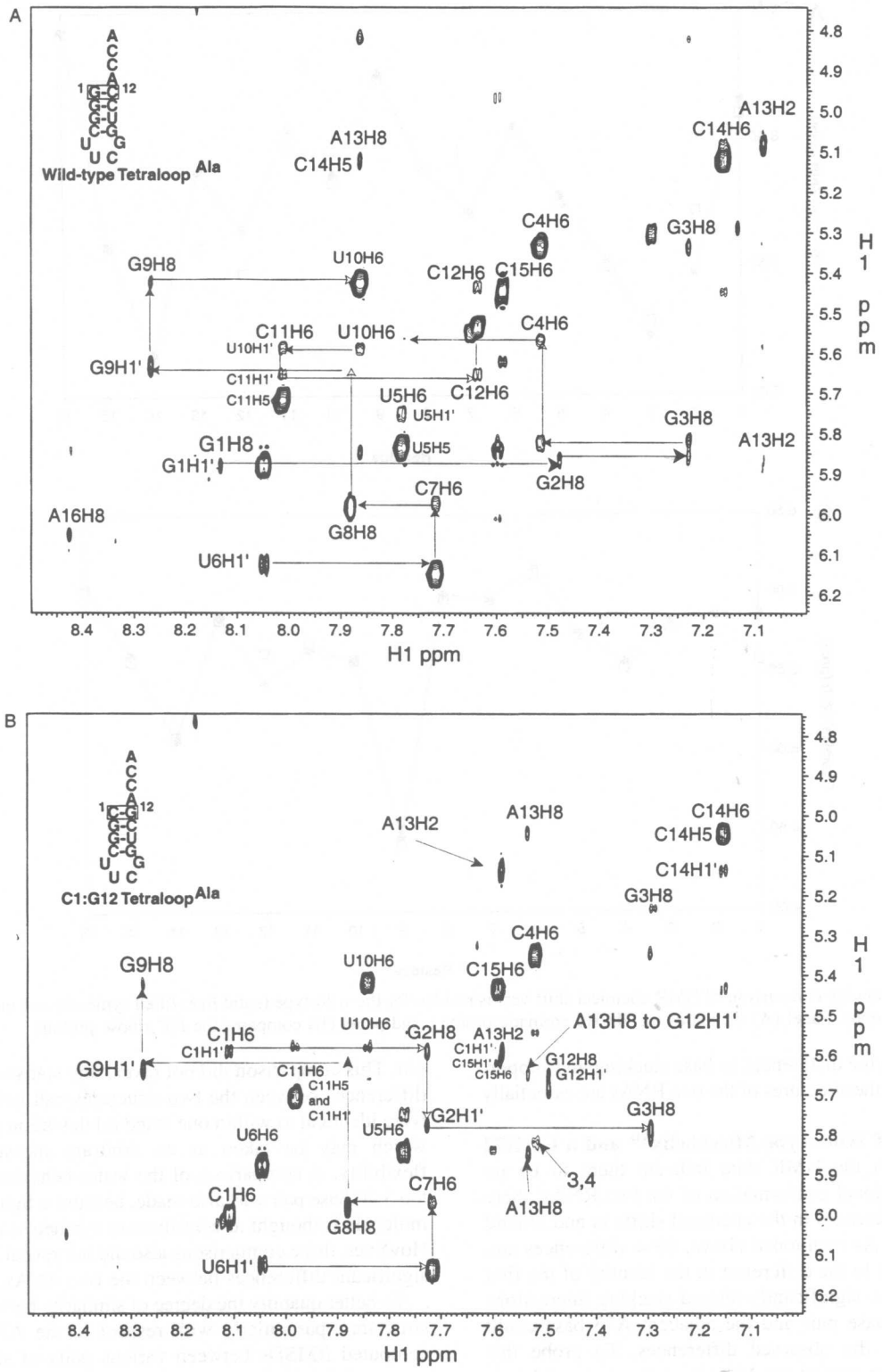


**Figure 2.** NOESY spectra at 800 MHz of (A) wild-type tetraloop$^{Ala}$ and (B) a C1:G12 variant. The spectra were recorded at 15 °C, and samples were at a concentration of 0.8 mM in 700 $\mu$L of NMR buffer.

shift is degenerate with the C15H1′ at most temperatures and fields. In addition, the chemical shift of G2H8 is altered from 7.48 ppm in the wild-type to 7.72 in the mutant. These chemical shift changes between the wild-type and mutant RNAs are consistent with the difference in the identity of the first base pair, which is a G:C in the wild-type versus a C:G in the mutant. The data do not support a significant conformational difference between the two RNAs but reflect differences in stacking of the discriminator base over the first base pair.

Protons not found in or adjacent to the first base pair show little sensitivity to it. A comparison of the aromatic and sugar H1′ chemical shifts versus residue number for the wild-type and mutant RNAs is shown in Figure 3. Overall, the chemical shift differences are consistent with globally similar structures, with the only significant changes occurring at or near the single base pair transversion. Excluding protons in A13 and the first two base pairs, the average $|\Delta\delta|$ for aromatic and sugar H1′ protons is only 0.03 ppm. Changes around the first base pair

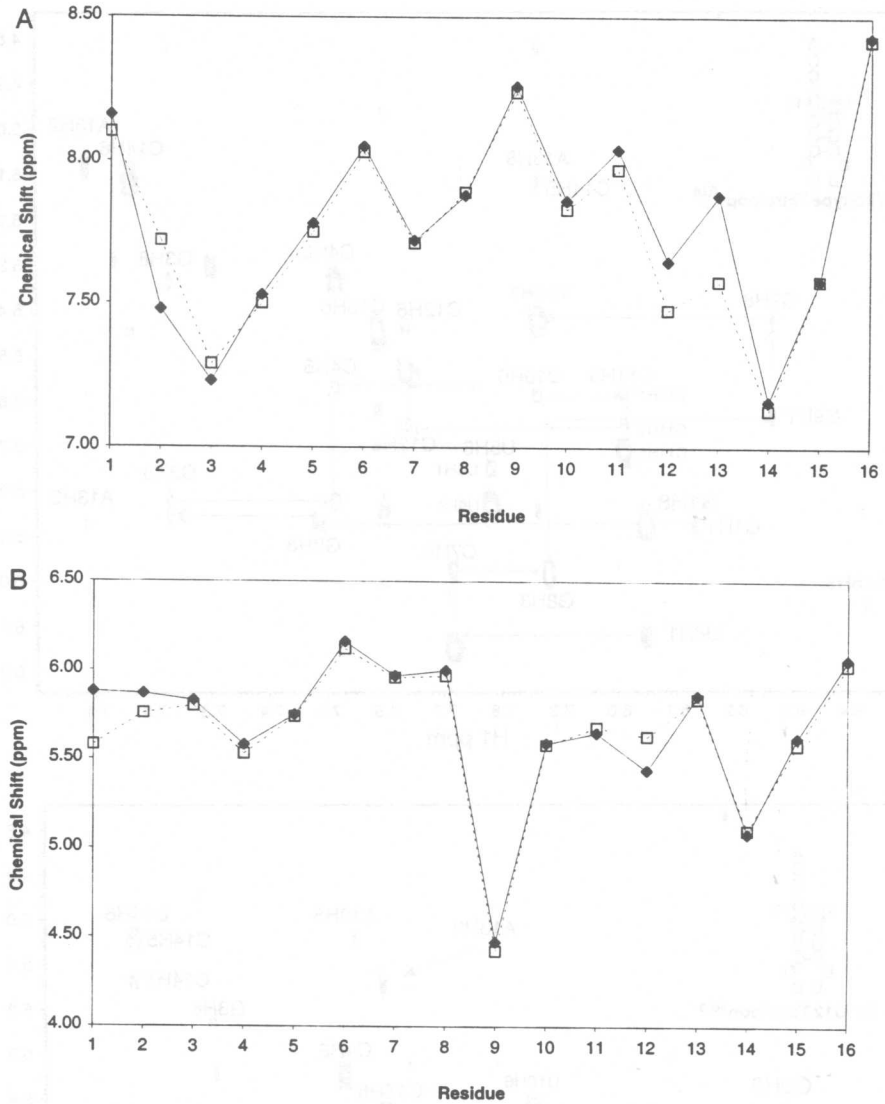


**Figure 3.** Graphs showing comparison of NMR chemical shift versus residue for the wild-type (solid line, filled symbols) and mutant (dotted line, open symbols) tetraloops. Panel (A) compares the H8/H6 aromatic protons, and panel (B) compares the H1′ ribose protons.

are consistent with the differences in base stacking and support the conclusion that the structures of the two RNAs are essentially the same.

**MD Analysis of Wild-Type Microhelix$^{Ala}$ and a C1:G72 Variant.** Although the NMR data indicate there to be no difference in the global conformation of the two RNAs, there are significant differences in the chemical shifts in and around the first base pair. As mentioned above, these differences are, at least in part, due to the difference in the identity of the first base pair. However, significantly altered stacking interactions between the first base pair and the adjacent A73 base could also contribute to the observed differences. To probe this question further, we carried out MD simulations on wild-type (2 trajectories) and mutant (1 trajectory) microhelices (Figure 1, right). The NMR structure of wild-type microhelix$^{Ala7}$ was the starting structure for the MD simulations and thus the longer 22-mer RNA framework was used to simulate the effect of the mutation as well. The root-mean-square deviations (RMSD) of each structure from its average over the 2-ns production-run period are shown in Figure 4 (RMSDs from starting structures are provided in Supporting Information). The small fluctuations in RMSDs indicate the systems to be statistically converged.[31,32] An exhaustive comparison of various average helical parameters[33,34] for the wild-type and mutant RNAs was next carried out. This comparison did not reveal any statistically significant differences between the two structures—all helical parameters were identical to within one standard deviation about the mean, which may be taken as an arbitrary measure of thermal flexibility. A comparison of the water behavior in and around the 3:70 base pair was also made, because a tightly bound water molecule is thought to contribute to synthetase recognition.[20,35] However, these comparisons also did not reveal any statistically significant differences between the two RNAs.

To better quantify the degree of similarity between the various structures, particularly with respect to the A73 location, we computed RMSDs between various pairs of structures. First, we examined the RMSD between the sequential 1-ns fragments of wild-type simulation A. The RMSD for all atoms in the microhelix excluding the CCA end (Table 1, column 2) is 0.62 Å. Much of this deviation can be attributed to flexibility in the tetraloop—when the RMSD is computed including only the double-helical region and including A73, the RMSD drops to 0.48 Å (Table 1, column 3). The RMSD contribution from A73 itself, 0.32 Å, is somewhat smaller than that from the double helix, 0.50 Å (Table 1, columns 4 and 5).

These values reflect the intrinsic flexibility of the microhelix within a single trajectory. To better estimate thermal noise, we also computed RMSDs by comparing the average structure for

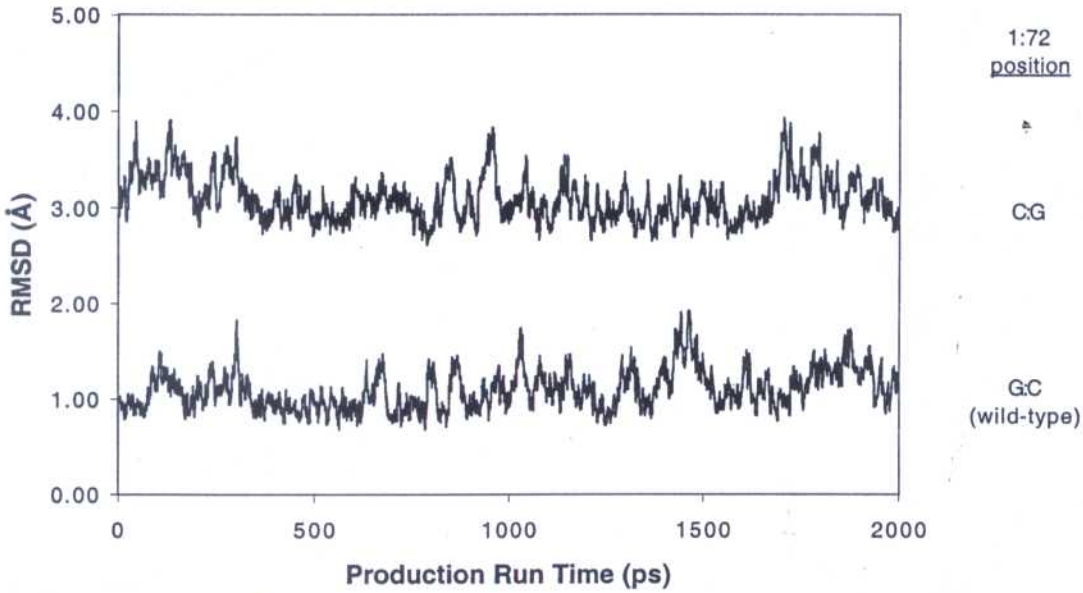


**Figure 4.** Root-mean-square deviations (Å) from average structures taken over the production run portion of each trajectory. Values have an arbitrary zero and are calculated excluding the single-stranded regions of the microhelices.

**TABLE 1: All-Atom RMSDs Compared to the Average Structure of the First 1 ns of Wild-Type Simulation A[a]**

| | residues involved in RMSD calculation | | | |
|---|---|---|---|---|
| structure compared | entire microhelix[b] | duplex + A73[c] | duplex[d] | A73[e] |
| wild-type A second 1 ns | 0.62 | 0.48 | 0.50 | 0.32 |
| wild-type B 1 ns | 1.00 | 0.83 | 0.72 | 1.65 |
| C1:G72 first 1 ns | 1.09 | 0.72 | 0.72 | 0.74 |
| C1:G72 second 1 ns | 0.90 | 0.63 | 0.63 | 0.62 |

[a] Based on optimal superposition of the conserved duplex regions (residues 2−7, and 66−71). [b] RMSDs calculated with residues 2−7, 66−71, 73, and the tetraloop. [c] RMSDs calculated with residues 2−7, 66−71, and 73. [d] RMSDs calculated with residues 2−7 and 66−71. [e] RMSDs calculated with residue 73.

the 1-ns wild-type B trajectory (started from a different random seed than the wild-type A trajectory) to the first 1 ns of the wild-type A trajectory. The RMSD values over the entire microhelix, duplex + A73, and duplex all increase by about 50% over those derived from comparison of the sequential fragments of simulation A. However, the RMSD over just A73 increases dramatically to 1.65 Å, indicating significant flexibility in the position of this base.

These numbers may be compared to RMSDs computed for the first and second 1-ns fragments of the C1:G72 simulation, again compared against the first 1 ns of wild-type A. In every comparison except for A73 alone, the RMSDs between wild-type A and mutant are quantitatively similar to those between wild-type A and wild-type B. In the case of the RMSD over just A73, the mutant structure shows *greater* similarity to wild-type A than does wild-type B, suggesting that there is no statistically significant difference in the location of A73 as a function of the 1:72 base pair.

A graphical analysis of this point is provided in Figure 5. Average structures in the figure have been superimposed using the heavy atoms of the first base pair riboses. There are only small differences in the relative position of A73 between all three structures, and what difference there is must be attributed to thermal noise. These analyses indicate that the dynamical

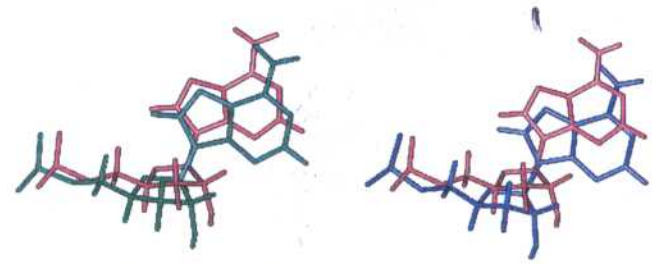

**Figure 5.** Comparison of the position of A73 based on the average structure obtained following 1 ns of MD simulation. The view is shown after superposition of the first base pair's ribose heavy atoms. On the left is shown a comparison of two different wild-type microhelix trajectories; on the right is a comparison of wild-type microhelix (red) to the C1:G72 mutant (blue).

position of A73 is not significantly different between the two RNAs.

The dynamic behavior of the A73 base was also characterized by monitoring the center of mass distance of the A73 base to a consistently defined fixed point in space. Snapshots of wild-type A, wild-type B and the mutant simulations obtained every 1 ps were superimposed upon the average structure obtained from the first picosedond of the wild-type A structure, using the heavy atoms of the first base pair riboses (fraying of this base pair was not observed in any simulation). Individual Cartesian components of the position as well as the overall distance were found to fluctuate consistently around average values (Supporting Information). The average positions of the A73 base in all simulations were found to be similar within a standard deviation (wild-type A, 4.2 ± 0.7 Å; wild-type B, 3.9 ± 0.5 Å; mutant, 3.4 ± 0.4 Å).

## Discussion

Previous NMR studies of tRNA acceptor stems have indicated that the solution conformation of the CCA-3′ end can be altered, depending on the identity of the discriminator base at position 73. For example, in the case of an *E. coli* $tRNA^{fMet}$ variant, a fold-back conformation for the CCA end is observed when the discriminator base is a U73, whereas an extended conformation is observed in the presence of A73.[12] The first base pair of the $microhelix^{fMet}$ variant used in this previous study was G1:C72.

The top part of the U73-containing microhelix$^{fMet}$ mimics the acceptor stem sequence of *E. coli* tRNA$^{Cys}$, and a subsequent NMR study confirmed a fold-back conformation for microhelix$^{Cys}$ as well.[14] The crystal structure of free *E. coli* initiator tRNA$^{fMet}$ also has a folded CCA end,[36,37] although an NMR study does not support this conclusion in solution.[13] This tRNA has an A73 and an unusual C1:A72 mismatch. A tRNA circularization assay has provided additional evidence that the solution conformation of the CCA end of tRNAs depends on the identity of N73 and the first base pair.[38] In particular, Hou and co-workers observed that the initial rate of tRNA circularization catalyzed by $T_4$ RNA ligase is fastest with pyrimidines at N73 and is also enhanced in the presence of a C1:A72 mismatch. In the context of *E. coli* tRNA$^{Cys}$, which has a G1:C72/U73 combination, a mutation to C1:G72 does not enhance the initial rate of circularization.[38]

The majority of X-ray crystallography and solution NMR studies of free tRNAs or microhelices containing A73 indicate that the CCA nucleotides are stacked on the end of the helix in an A-form conformation.[7,12,13,39–42] Of particular relevance to the present study, the solution NMR structure of microhelix$^{Ala}$ showed that it has an extended CCA end and that the A73 discriminator base stacks predominantly onto G1 of the first base pair.[7,41] Biochemical studies and MD simulations support the conclusion that this stacking interaction is important for aminoacylation activity.[6,8] Given the striking effect that mutations at position 1:72 have on aminoacylation by AlaRS,[9–11,43] and the evidence that the identity of this base pair can alter the conformational flexibility of the CCA end of tRNAs in general, the solution structure of the inactive C1:G72 variant is an important new datum. Both our NMR and our MD results indicate that the global fold of the ACCA-3′ end in the inactive C1:G72-containing acceptor stem is *not* different from that of the wild-type RNA. Thus, this acceptor stem represents another context wherein the CCA end maintains a stacked, A-form helix. The NMR and MD simulation results further indicate that the position of A73, a well-known determinant for aminoacylation by AlaRS, is not significantly affected by the base pair transversion (Figure 5).

We previously showed that the 6-keto oxygen of G72 blocks in vitro aminoacylation with alanine. In particular, an extensive biochemical analysis showed that the negative effect of N1:G72 (where N is any nucleotide) base pairs could be substantially relieved by incorporation of N1:2-aminopurine (N1:2AP). These studies showed that the presence of the 6-keto oxygen and N1 proton of G72 contributes at least 3.0 kcal/mol to transition state stabilization.[10] The new conformational studies reported here allow us to understand the mechanism of this blocking effect better. Because 1:72 base pair transversion results in neither a global nor a significant local conformational change nor does it influence the dynamics of A73 base stacking, the atomic groups of G72 appear to have a direct effect on blocking recognition by AlaRS.

The conformation of the acceptor stem of tRNA$^{Ala}$ bound to AlaRS is unknown. However, there is evidence in other tRNA–protein systems that significant conformational changes in the CCA end can occur upon binding.[44–46] This kind of induced-fit mechanism is a key feature of tRNA–synthetase recognition.[47] Our results show that, in the initial contact made by AlaRS, the enzyme is likely to encounter a very similar conformation of the G1:C72 and C1:G72 acceptor stems. Indeed, the C1:G72 duplex$^{Ala}$ binds to AlaRS, as evidenced by the inhibition of wild-type tRNA$^{Ala}$ aminoacylation.[10] The new data presented in this work suggests that the negative effect of a C1:G72 mutation results in an unfavorable protein–RNA interaction at this base pair, which is proximal to the catalytic site. For example, the presence of the 6-keto oxygen of G72 alters the local electrostatic potential in the major groove, and this may render the induced fit required to form the properly bound complex necessary for efficient aminoacylation less energetically favorable.

**Acknowledgment.** We thank the American Chemical Society-Petroleum Research Fund, the Minnesota Supercomputer Institute, the National Institutes of Health, and the Alfred P. Sloan Foundation for financial support. We also acknowledge the University of Minnesota NMR center, which is partially supported by the National Science Foundation. M.C.N., P.J.B. and M.R.T. received support from a National Institutes of Health Molecular Biophysics training grant and the American Foundation for Pharmaceutical Education (M.R.T.).

**Supporting Information Available:** The Supporting Information includes helical parameters and RMSDs from starting structures used to assess convergence of simulations. A table of proton chemical shift data for the C1:G12 tetraloop$^{Ala}$ is provided and A73 base position fluctuations over time are also given. This material is free of charge via the Internet at http://pubs.acs.org.

## References and Notes

(1) Giegé, R.; Sissler, M.; Florentz, C. *Nucl. Acids Res.* **1998**, *26*, 5017.
(2) Hou, Y.-M.; Schimmel, P. *Nature* **1988**, *333*, 140.
(3) McClain, W. H.; Chen, Y.-M.; Foss, K.; Schneider, J. *Science* **1988**, *242*, 1681.
(4) Musier-Forsyth, K.; Usman, N.; Scaringe, S.; Doudna, J.; Green, R.; Schimmel, P. *Science* **1991**, *253*, 784.
(5) Musier-Forsyth, K.; Schimmel, P. *Nature* **1992**, *357*, 513.
(6) Fischer, A. E.; Beuning, P. J.; Musier-Forsyth, K. *J. Biol. Chem.* **1999**, *274*, 37093.
(7) Ramos, A.; Varani, G. *Nucl. Acids Res.* **1997**, *25*, 2083.
(8) Nagan, M. C.; Beuning, P.; Musier-Forsyth, K.; Cramer, C. J. *Nucl. Acids Res.* **2000**, *28*, 2527.
(9) Liu, H.; Kessler, J.; Peterson, R.; Musier-Forsyth, K. *Biochemistry* **1995**, *34*, 9795.
(10) Beuning, P. J.; Gulotta, M.; Musier-Forsyth, K. *J. Am. Chem. Soc.* **1997**, *119*, 8397.
(11) Liu, H.; Yap, L.-P.; Musier-Forsyth, K. *J. Am. Chem. Soc.* **1996**, *118*, 2523.
(12) Puglisi, E. V.; Puglisi, J. D.; Williamson, J. R.; RajBhandary, U. L. *Proc. Natl. Acad. Sci. U.S.A.* **1994**, *91*, 11467.
(13) Zuleeg, T.; Vogtherr, M.; Schubel, H.; Limmer, S. *FEBS Lett.* **2000**, *472*, 247.
(14) Hou, Y.-M.; Zhang, X.; Holland, J. A.; Davis, D. R. *Nucl. Acids Res.* **2001**, *29*, 971.
(15) Maniatis, T.; Fritsch, E. F.; Sambrook, J. *Molecular Cloning: A Laboratory Manual*; Cold Spring Harbor Laboratory Press: Cold Spring Harbor, NY, 1982.
(16) Scaringe, S. A.; Francklyn, C.; Usman, N. *Nucl. Acids Res.* **1990**, *18*, 5433.
(17) Sproat, B.; Colonna, F.; Mullah, B.; Tsou, D.; Andrus, A.; Hampel, A.; Vinayak, R. *Nucleosides & Nucleotides* **1995**, *14*, 255.
(18) Beuning, P. J.; Tessmer, M. R.; Baumann, C. G.; Kallick, D. A.; Musier-Forsyth, K. *Anal. Biochem.* **1999**, *273*, 284.
(19) States, D. J.; Haberkorn, R. A.; Ruben, D. J. *J. Magn. Reson.* **1982**, *48*, 286.
(20) Nagan, M. C.; Kerimo, S. S.; Musier-Forsyth, K.; Cramer, C. J. *J. Am. Chem. Soc.* **1999**, *121*, 7310.
(21) Cornell, W. D.; Cieplak, P.; Bayly, C. I.; Gould, I. R.; Merz, K. M., Jr.,; Ferguson, D. M.; Spellmeyer, D. C.; Fox, T.; Caldwell, J. W.; Kollman, P. A. *J. Am. Chem. Soc.* **1995**, *117*, 5179.
(22) Case, D. A.; Pearlman, D. A.; Caldwell, J. W.; Cheatham, T. E., III; Ross, W. S.; Simmerling, C. L.; Darden, T. A.; Merz, K. M.; Stanton, R. V.; Cheng, A. L.; Vincent, J. J.; Crowley, M.; Ferguson, D. M.; Radmer, R. J.; Seibel, G. L.; Singh, U. C.; Weiner, P. K.; Kollman, P. A. *AMBER*, 5.0 ed.; University of California: San Francisco, CA, 1997.
(23) Jorgensen, W. L.; Chandreskhar, J.; Madura, J. D.; Impey, R. W.; Klein, J. *J. Chem. Phys.* **1983**, *79*, 926.

(24) York, D. M.; Darden, T. A.; Pedersen, L. G. *J. Chem. Phys.* **1993**, *99*, 8345.

(25) Ryckaert, J. P.; Ciccotti, G.; Berendsen, H. J. C. *J. Comput. Phys.* **1977**, *23*, 327.

(26) Berendsen, H. J. C.; Postma, J. P. M.; van Gunsteren, W. F.; A. DiNola, A.; Haak, J. R. *J. Comput. Phys.* **1984**, *81*, 3684.

(27) Cheatham, T. E., III; Kollman, P. A. *J. Am. Chem. Soc.* **1997**, *119*, 4805.

(28) Lavery, R.; Skelnar, H. *Curves*, 5.3 ed.; Institut de Biologie Physico-Chimique: Paris, France, 1998.

(29) *InsightII*, 98.0 ed.; Molecular Simulations, Inc.: San Diego, CA, 2000.

(30) Humphrey, W.; Dalke, A.; Schulten, K. *J. Mol. Graph* **1996**, *14*, 33.

(31) Cheatham, T. E., III; Brooks, B. R. *Theor. Chem. Acc.* **1998**, *99*, 279.

(32) Cheatham, T. E., III; Kollman, P. A. Molecular dynamics simulation of nucleic acids in solution: how sensitive are the results to small perturbations in the force field and environment? In *Structure, Motion, Interaction, and Expression of Biological Macromolecules*; Sarma, R. H., Sarma, M. H., Eds.; Adenine Press: New York, 1998; p 99.

(33) Lavery, R.; Sklenar, H. *J. Biomol. Struct. Dynam.* **1988**, *6*, 63.

(34) Lavery, R.; Sklenar, H. *J. Biomol. Struct. Dynam.* **1989**, *6*, 655.

(35) Mueller, U.; Schübel, H.; Sprinzl, M.; Heinemann, U. *RNA* **1999**, *5*, 670.

(36) Schevitz, R. W.; Podjarny, A. D.; Krishnamachari, N.; Hughes, J. J.; Sigler, P. B.; Sussman, J. L. *Nature* **1979**, *278*, 188.

(37) Woo, N. H.; Roe, B. A.; Rich, A. *Nature* **1980**, *286*, 346.

(38) Hou, Y.-M.; Lipman, R. S. A.; Zarutskie, J. A. *RNA* **1998**, *4*, 733.

(39) Robertus, J. D.; Ladner, J. E.; Finch, J. T.; Rhodes, D.; Brown, R. S.; Clark, B. F. C.; Klug, A. *Nature* **1974**, *250*, 546.

(40) Kim, S. H.; Suddath, F. L.; Quigley, G. J.; McPherson, A.; Sussman, J. L.; Wang, A. H. J.; Seeman, N. C.; Rich, A. *Science* **1974**, *185*, 435.

(41) Limmer, S.; Hofmann, H.-P.; Ott, G.; Sprinzl, M. *Proc. Natl. Acad. Sci. U.S.A.* **1993**, *90*, 6199.

(42) Metzger, A. U.; Heckl, M.; Willbold, D.; Bretschopf, K.; RajBhandary, U. L.; Rösch, P.; Gross, H. J. *Nucl. Acids Res.* **1997**, *25*, 4551.

(43) McClain, W. H.; Foss, K.; Jenkins, R. A.; Schneider, J. *Proc. Natl. Acad. Sci. U.S.A.* **1991**, *88*, 9272.

(44) Rould, M. A.; Perona, J. J.; Söll, D.; Steitz, T. A. *Science* **1989**, *246*, 1135.

(45) Silvian, L. F.; Wang, J.; Steitz, T. A. *Science* **1999**, *285*, 1074.

(46) Madore, E.; Lipman, R. S. A.; Hou, Y.-M.; Lapointe, J. *Biochemistry* **2000**, *39*, 6791.

(47) Cusack, S. *Curr. Opin. Struct. Biol.* **1998**, *7*, 8881.